

Calculation of HELAS amplitudes for QCD processes using graphics processing unit (GPU)

K. Hagiwara¹, J. Kanzaki^{2,a}, N. Okamura^{2,b}, D. Rainwater³, and T. Stelzer^{4,c}

¹ KEK Theory Center and Sokendai, Tsukuba 305-0801, Japan

² KEK, Tsukuba 305-0801, Japan

³ Space and Geophysics Laboratory, Applied Research Laboratories, University of Texas, Austin, TX 78758, USA

⁴ Dept. of Physics, University of Illinois, Urbana, IL, USA

Received: date / Revised version: October 21, 2018

Abstract. We use a graphics processing unit (GPU) for fast calculations of helicity amplitudes of quark and gluon scattering processes in massless QCD. New HEGET (**HELAS Evaluation with GPU Enhanced Technology**) codes for gluon self-interactions are introduced, and a C++ program to convert the MadGraph generated FORTRAN codes into HEGET codes in CUDA (a C-platform for general purpose computing on GPU) is created. Because of the proliferation of the number of Feynman diagrams and the number of independent color amplitudes, the maximum number of final state jets we can evaluate on a GPU is limited to 4 for pure gluon processes ($gg \rightarrow 4g$), or 5 for processes with one or more quark lines such as $q\bar{q} \rightarrow 5g$ and $qq \rightarrow qq+3g$. Compared with the usual CPU-based programs, we obtain 60-100 times better performance on the GPU, except for 5-jet production processes and the $gg \rightarrow 4g$ processes for which the GPU gain over the CPU is about 20.

1 Introduction

In our previous report [1] we introduced a C-language [2] version of the HELAS codes [3], HEGET (**HELAS Evaluation with GPU Enhanced Technology**), which can be used to compute helicity amplitudes on a GPU (Graphics Processing Unit). Encouraging results with 40-150 times faster computation speed over the CPU performance were obtained for pure QED processes, $q\bar{q} \rightarrow n\gamma$, for $n=2$ to 8 in pp collisions.

In this paper, we extend our study to QCD processes with massless quarks and gluons. The HEGET routines for massless quarks and gluons are identical to those of quarks and photons introduced in [1], and the qqg vertex function structure is also the same as the $qq\gamma$ functions. The only new additional routines are those for ggg and $gggg$ vertices. For the QED processes studied in ref. [1], we found that the present CUDA compiler cannot process $q\bar{q} \rightarrow 6\gamma$ amplitude with $6! \approx 700$ Feynman diagrams, and we need to subdivide the HEGET codes into small pieces for 6γ and 7γ processes. In the case of 8γ production with $8! \approx 4 \times 10^4$ Feynman diagrams, we have not been able to compile the program even after subdivision into small pieces. We also encountered serious slow down when the program accesses global memory during the parallel processing period. Therefore, our concern for evaluating the

QCD processes on a GPU is the proliferation of the number of diagrams, as well as the number of independent color amplitudes which come with different color weights.

The paper is organized as follows. In section 2, we present the cross section formula for n -jet production processes in pp collisions in the quark-parton model, or in the leading order of perturbative QCD with scale-dependent parton distribution functions (PDF's). In section 3, we review briefly the structure of GPU computing by using HEGET codes, and give basic parameters of the GPU and CPU machines used in this analysis. In section 4, we introduce new HEGET functions for ggg and $gggg$ vertices. Section 5 gives our results and section 6 summarizes our findings. Appendix lists all the new HEGET codes introduced in section 4.

2 Physics Process

2.1 n -jet production in pp collisions

The cross section for n -jet production processes can be expressed as

$$d\sigma = \sum_{\{a,b\}} \iint dx_a dx_b D_{a/p}(x_a, Q) D_{b/p}(x_b, Q) d\hat{\sigma}(\hat{s}), \quad (1)$$

where $D_{a/p}$ and $D_{b/p}$ are the scale (Q) dependent parton distribution functions (PDF's), x_a and x_b are the momentum fractions of the partons a and b , respectively, in the

^a e-mail: junichi.kanzaki@kek.jp

^b e-mail: naotoshi@post.kek.jp

^c e-mail: tstelzer@uiuc.edu

Table 1. The number of Feynman diagrams and the color bases for QCD processes studied in this paper.

No. of jets in the final state	$gg \rightarrow$ gluons		$u\bar{u} \rightarrow$ gluons		$uu \rightarrow uu +$ gluons	
	#diagrams	#colors	#diagrams	#colors	#diagrams	#colors
2	6	6	3	2	2	2
3	45	24	18	6	10	8
4	510	120	159	24	76	40
5	7245	720	1890	120	786	240

right- and left-moving protons. For the total pp collision energy of \sqrt{s} ,

$$\hat{s} = s x_a x_b, \quad (2)$$

gives the invariant mass squared of the hard collision process

$$\mathbf{a} + \mathbf{b} \rightarrow \mathbf{1} + \mathbf{2} + \cdots + \mathbf{n}. \quad (3)$$

The subprocess cross section is computed in the leading order as

$$d\hat{\sigma}(\hat{s}) = \frac{1}{2\hat{s}} \frac{1}{2 \cdot 2} \sum_{\lambda_i} \frac{1}{n_a n_b} \sum_{c_i} |\mathcal{M}_{\lambda_i}^{c_i}|^2 d\Phi_n, \quad (4)$$

where

$$d\Phi_n = (2\pi)^4 \delta^4 \left(p_a + p_b - \sum_{i=1}^n p_i \right) \prod_{i=1}^n \frac{d^3 p_i}{(2\pi)^3 2\omega_i}, \quad (5)$$

is the invariant n -body phase space, λ_i are the helicities of the initial and final partons, n_a and n_b are the color degree of freedom of the initial partons, a and b , respectively, and c_i represents the color indices of the initial and final partons. When there are more than one gluons or identical quarks in the final states, an appropriate statistical factor should be multiplied on the phase space $d\Phi_n$ in eq. (5).

The Helicity amplitudes for the process (1)

$$\begin{aligned} & \mathbf{a}(p_a, \lambda_a, c_a) + \mathbf{b}(p_b, \lambda_b, c_b) \\ & \rightarrow \mathbf{1}(p_1, \lambda_1, c_1) + \cdots + \mathbf{n}(p_n, \lambda_n, c_n) \end{aligned} \quad (6)$$

can be expressed as

$$\mathcal{M}_{\lambda_i}^{c_i} = \sum_{l \in \text{diagram}} (M_{\lambda_i})_l^{c_i} \quad (7)$$

where the summation is over all the Feynman diagrams. The subscripts λ_i stand for a given combination of helicities (± 1 for both quarks and gluons in the HELAS convention [3]), and the subscripts c_i correspond to a set of color indices (1, 2, 3 for flowing-IN quarks, $\bar{1}, \bar{2}, \bar{3}$ for flowing-OUT quarks, and 1 to 8 for gluons). In MadGraph [4] the amplitudes are expanded as

$$\mathcal{M}_{\lambda_i}^{c_i} = \sum_{\alpha} T_{\alpha}^{c_i} (J_{\lambda_i})_{\alpha} \quad (8)$$

in the color bases $T_{\alpha}^{c_i}$ which are made from the SU(3) generators in the fundamental representation [5]

The color factors are computed as

$$\mathcal{N}_{\alpha\beta} = \frac{1}{n_a n_b} \sum_{c_i} (T_{\alpha}^{c_i}) (T_{\beta}^{c_i})^* \quad (9)$$

where $n_{a,b} = 3$ for q and \bar{q} , $n_{a,b} = 8$ for gluons, and the summation is over all $\{c_i\} = \{c_a, c_b, c_1, \dots, c_n\}$. The color sum-averaged square amplitudes are computed as

$$\overline{\sum_{c_i} |\mathcal{M}_{\lambda_i}^{c_i}|^2} = \sum_{a,b} (J_{\lambda_i})_{\alpha} \mathcal{N}_{\alpha\beta} (J_{\lambda_i})_{\beta}^*. \quad (10)$$

The cross sections are then expressed as

$$d\hat{\sigma}(\hat{s}) = \frac{1}{2\hat{s}} \overline{\sum_{\lambda_i} \sum_{c_i} |\mathcal{M}_{\lambda_i}^{c_i}|^2} d\Phi_n, \quad (11)$$

where we introduce the helicity sum-average symbol as

$$\overline{\sum_{\lambda_i}} \equiv \frac{1}{2} \frac{1}{2} \sum_{\lambda_i}. \quad (12)$$

In this paper the following three types of multi-jet production processes are computed:

$$gg \rightarrow gg, ggg, gggg \quad (13a)$$

$$q\bar{q} \rightarrow gg, ggg, gggg, ggggg \quad (13b)$$

$$uu \rightarrow uu, uug, uugg, uuggg \quad (13c)$$

The number of contributing Feynman diagrams and the number of color bases for the above processes are summarized in Table 1, which includes those for the process, $gg \rightarrow 5g$. We note here that the number of diagrams (7245) for $gg \rightarrow 5g$ exceeds that of the $u\bar{u} \rightarrow 7\gamma$ process ($7! \approx 5040$), for which we could run the converted MadGraph codes on a GPU, only after division into small pieces [1]. In fact, we have not been able to run the $gg \rightarrow 5g$ program on GPU even after dividing the program into more than 100 pieces; as explained in section 5.4.

Proliferation of the number of independent color basis vectors is also a serious concern for GPU computing, since the color matrix \mathcal{N} of eq. (9) has $m(m+1)/2$ elements when there are m independent basis vectors $T_{\alpha}^{c_i}$. For example, the process $uu \rightarrow uuggg$ has $m = 240$ color basis vectors from Table 1, and the matrix has 3×10^4 elements. The matrix exceeding 16000 elements cannot be stored in the 64kB constant memory, while storing it in the global memory will result in serious loss of efficiency in parallel computing. Therefore, the method to handle summation over color degrees of freedom is a serious concern in GPU computing.

2.2 Selection criteria for jets

Total and differential cross sections of the processes (13) in pp collisions at $\sqrt{s}=14\text{TeV}$ are computed in this paper. We introduce final state cuts for all the jets as follows:

$$|\eta_i| < \eta^{\text{cut}} = 2.5, \quad (14a)$$

$$p_{T_i} > p_T^{\text{cut}} = 20 \text{ GeV}, \quad (14b)$$

$$p_{T_{ij}} > p_T^{\text{cut}} = 20 \text{ GeV}, \quad (14c)$$

where η_i and p_{T_i} are the rapidity and the transverse momentum of the i -th jet, respectively, in the pp collisions rest frame along the right-moving ($p_z = |p|$) proton momentum direction, and $p_{T_{ij}}$ is the relative transverse momentum [6] between the jets i and j defined by

$$p_{T_{ij}} \equiv \min(p_{T_i}, p_{T_j}) \Delta R_{ij}, \quad (15a)$$

$$\Delta R_{ij} = \sqrt{\Delta\eta_{ij}^2 + \Delta\phi_{ij}^2}. \quad (15b)$$

Here ΔR_{ij} measures the boost-invariant angular separation between the jets.

As for the parton distribution function (PDF), we use the set CTEQ6L1 [7] and the factorization scale is chosen to be the cut-off p_T value, $Q = p_T^{\text{cut}} = 20 \text{ GeV}$. The QCD coupling constant is also fixed as

$$\alpha_s = \alpha_s(Q=20\text{GeV})_{\overline{\text{MS}}} = 0.171, \quad (16)$$

which is obtained from the $\overline{\text{MS}}$ coupling at $Q = m_Z$, $\alpha_s(m_Z)_{\overline{\text{MS}}} = 0.118$ [8] by using the NLO renormalization group equations with 5-flavors.

3 Computation on the GPU

3.1 GPU and its host PC

For the computation of the cross sections of QCD n -jet production processes we use the same GPU and host PC as in the previous report [1]. In particular we use a GeForce GTX280 by NVIDIA [11] with 240 processors, whose parameters are summarized in Table 2. It is controlled by a Linux PC with Fedora 8 on a CPU whose properties are summarized in Table 3.

Programs which are used for the computation of the cross sections are developed with the CUDA [2] environment introduced by NVIDIA [11] for general purpose GPU computing.

3.2 Program structure

Our program computes the total cross sections and distributions of the QCD n -jet production processes via the following procedure:

1. initialization of the program,
2. random number generation for multiple phase-space points $\{p_a, p_b, p_1, \dots, p_n\}$ and helicities $\{\lambda_i\}$ on the CPU,

Table 2. Parameters of GeForce GTX280.

Number of multiprocessor	30
Number of core	240
Total amount of global memory [MB]	1000
Total amount of constant memory [kB]	64
Total amount of shared memory per block [kB]	16
Total number of registers available per block [kB]	16
Clock rate [GHz]	1.30

Table 3. Host PC environment.

CPU	Core2Duo 3GHz
L2 Cache	6MB
Memory	4GB
Bus Speed	1.333GHz
OS	Fedora 8 (64 bit)

3. transfer of random numbers to the GPU,
4. generation of helicities and momenta of initial and final partons using random numbers, and compute amplitudes $(J_{\lambda_i})_a$ of eq. (8) for all the color bases on the GPU,
5. multiplying the amplitudes and their complex conjugate with the color matrix \mathcal{N}_{ab} of eq. (9) and summing them up as in eq. (10), and multiply the PDF's of the incoming partons on the GPU,
6. transferring momenta and helicities for external particles, computed weights and the color summed squared amplitudes to the CPU, and
7. summing up all values to obtain the total cross section and distributions on the CPU.

Program steps between the generation of random numbers (2) and the summation of computed cross sections (7) are repeated until we obtain sufficient statistics for the cross section and all distributions.

3.3 Color matrix calculation

In order to compute the cross sections of the QCD multi-jet production processes, multiplications of the large color matrix \mathcal{N}_{ab} of eq. (9), the vector of color-bases amplitudes $(J_{\lambda_i})_\alpha$ of eq. (8) and its complex conjugate have to be performed, as in eq. (10). For large n -jet processes, like $gg \rightarrow 4$ gluons, $u\bar{u} \rightarrow 5$ gluons and $uu \rightarrow uu + 3$ gluons, the dimensions of color matrices exceed 100, and the number of multiplication becomes larger than 10^4 . These matrices cannot be stored in the constant memory (64kB for the GTX280; see Table 2) which is accessed in parallel, while storing them in the global memory (1GB for GTX280) results in serious slow-down of the GPU. We find that multiplications for the color-summation in eq. (10) can be reduced significantly as follows.

Table 4. Number of different non-zero elements in the color matrix of eq. (9).

No. of jets	$gg \rightarrow$ gluons	$u\bar{u} \rightarrow$ gluons	$uu \rightarrow uu +$ gluons
2	3	2	2
3	7	4	7
4	15	9	19
5	45	24	60

The color matrix of eq. (9) contains many elements with the same value. We count the number of different non-zero elements in the color matrix and find the results shown in Table 4. We find for instance that among the $240 \times (240+1)/2 = 28,720$ elements of the color matrix for the $uu \rightarrow uu + 3g$ process, there are only 60 unique ones.

In general, the number of different elements in the color matrix grows linearly rather than quadratically as the number of color basis vectors grows. Since the numbers in Table 4 are small enough, we can store them in the constant memory which is accessed quickly by each parallel processor.

Before we arrive at the above solution adopted in this study, we examined the possibility of summing over colors via Monte Carlo. Let us briefly report, in passing, on this exercise.

In the Monte Carlo color summation approach, we evaluate the matrix element $\mathcal{M}_{\lambda_i}^{c_i}$ (7) for a given set of momenta $\{p_i\}$, helicities $\{\lambda_i\}$ and colors $\{c_i\}$, and sum the squared amplitudes over randomly generated sets of $\{p_i, \lambda_i, c_i\}$. This method turns out not to be efficient because in the color basis using the fundamental representation of the SU(3) generators adopted by MadGraph, most of the basis vectors $T_a^{c_i}$ vanish for a given color configuration $\{c_i\}$. As an example, $gg \rightarrow 4g$ has $5! = 120$ color basis vectors (see Table 1), which take the form

$$T_a^{c_i} = \text{Tr}(T^{a_1} T^{a_2} \dots T^{a_6}) \quad (17)$$

for the configuration $\{c_i\} = (a_1, a_2, \dots, a_6)$ where a_i denotes the color index of the gluon i taking an integer value between 1 and 8. Among the $8^6 \approx 260,000$ configurations, only 12% give non-zero values. Moreover, as many as 75% of the color configurations give vanishing results for all the 120 basis vectors. Although the efficiency can be improved by changing the color basis, we find that our solution of evaluating the exact summation over colors is superior to the Monte Carlo summation method for all the processes which we report in this paper.

4 New HEGET functions

The HEGET functions for massless quarks and gluons are the same as those introduced in the previous report [1]. The qqg vertex functions are identical to the $qq\gamma$ functions of ref. [1] except for the coupling constant;

$$eQ_q \rightarrow g_s T_{ij}^a \quad (18)$$

for the vertex

$$\mathcal{L}_{qqg} = -g_s T_{ij}^a A_\mu^a(x) \bar{q}_i(x) \gamma_\mu q_j(x) \quad (19)$$

where $g_s = \sqrt{4\pi\alpha_s}$ is the strong coupling constant and T_{ij}^a is an SU(3) generator in the fundamental representation. For example, the qqg vertex function is computed by the HEGET function `iovxx0` as

```
iovxx0(cmplx* fi, cmplx* fo, cmplx* vc, float g,
      cmplx vertex)
(20)
```

where the coupling constants are

$$g[0] = g[1] = g_s \quad (21)$$

following the convention of MadGraph [4] and the color amplitude is ¹

$$-T_{ij}^a(\mathbf{vertex}). \quad (22)$$

In the rest of this section, we introduce new HEGET functions for three-vector boson (VVV) and four-vector boson (VVVV) vertices. All the new HEGET functions are listed in Table 5, and their contents are given in Appendix. Also shown in Table 5 is the correspondence between the HEGET functions and the HELAS subroutines [3].

4.1 VVV: three vector boson vertex

For the ggg vertex

$$\mathcal{L}_{ggg} = g_s f^{abc} (\partial^\mu A^{a\nu}(x)) A_\mu^b(x) A_\nu^c(x) \quad (23)$$

we introduce two HEGET functions, `vvvxxx` and `jvvxxx0`. They correspond to HELAS subroutines, `VVVXXX`, and `JVVXXX`, respectively, for massless particles; see Table 5.

4.1.1 vvvxxx

The HEGET function `vvvxxx` (List 1 in Appendix) computes the amplitude of the VVV vertex from vector boson wave functions, whether they are on-shell or off-shell. The function has the arguments:

```
vvvxxx(cmplx* ga, cmplx* gb, cmplx* gc,
      float g, cmplx vertex)
(24)
```

where the inputs and the outputs are:

INPUTS:

```
cmplx ga[6]  wavefunction of gluon with color
              index, a
cmplx gb[6]  wavefunction of gluon with color
              index, b
cmplx gc[6]  wavefunction of gluon with color
              index, c
float g      coupling constant of VVV vertex
(25)
```

OUTPUTS:

```
cmplx vertex amplitude of the VVV vertex
```

¹ The sign of the color amplitudes (22) and (27) follows the sign of the Lagrangian terms (19) and (23), respectively. MadGraph [4] adopts the Lagrangian with the opposite sign, that is, $(g_s)_{\text{MadGraph}} = -g_s$. This sign difference is absorbed by the conventions (22) and (27).

Table 5. List of the new vertex functions in HEGET.

Vertex	Inputs	Output	HEGET Function	HELAS Subroutine
VVV	VVV VV	Amplitude V	vvvxxx jvvxx0	VVVXXX JVVXXX
VVVV	GGGG GGG	Amplitude G	ggggxx jgggx0	GGGGXX JGGGXX

The coupling constant is

$$g = g_s \quad (26)$$

in the HEGET function (24), following the convention of MadGraph [4]. In order to reproduce the amplitudes associated with the ggg vertex Lagrangian of eq. (23), the color factor associated with the ggg vertex is if^{abc} . More explicitly, the vertex amplitude for eq. (23) is¹

$$if^{abc}(\mathbf{vertex}) \quad (27)$$

by using the output (**vertex**) in eq. (24). Also note the HELAS convention [3] of using the flowing-OUT momenta and quantum numbers for all bosons.

4.1.2 jvvxx0

This HEGET function `jvvxx0` (List 2 in Appendix) computes the off-shell vector wavefunction from the three-point gauge boson coupling in eq. (23). The vector propagator is given in the Feynman gauge for a massless vector bosons like gluons. It has the arguments:

$$\text{jvvxx0}(\text{cplx* ga}, \text{cplx* gb}, \text{float g}, \text{cplx* jvv}) \quad (28)$$

where the inputs and the outputs are:

INPUTS:

`cplx ga[6]` wavefunction of gluon with color index, a
`cplx gb[6]` wavefunction of gluon with color index, b
`float g` coupling constant of the VVV vertex

OUTPUTS:

`cplx jvv[6]` vector current $j^\mu(\mathbf{gc}:\mathbf{ga},\mathbf{gb})$ which has a color index, c (29)

As in eq. (27) the color amplitude for the off-shell current is

$$if^{abc}(\mathbf{jvv}). \quad (30)$$

4.2 VVVV: four vector boson vertex

For the $gggg$ vertex

$$\mathcal{L}_{gggg} = -\frac{g_s^2}{4} f^{abe} f^{cde} A^{\mu}(x) A^{\nu}(x) A_{\mu}^c(x) A_{\nu}^d(x) \quad (31)$$

we introduce two HEGET functions, `ggggxx` and `jgggx0`, listed in Table 5. They correspond to HELAS subroutines, `GGGGXX` and `JGGGXX`, respectively, for massless particles.

4.2.1 ggggxx

The HEGET function `ggggxx` (List 3 in Appendix) computes the portion of the amplitude of the $gggg$ amplitude where the first and the third, and hence also, the second and the fourth gluon wave functions are contracted, whether the gluons are on-shell or off-shell. The function has the arguments:

$$\text{ggggxx}(\text{cplx* ga}, \text{cplx* gb}, \text{cplx* gc}, \text{cplx* gd}, \text{float g}, \text{cplx vertex}) \quad (32)$$

where the inputs and the outputs are:

INPUTS:

`cplx ga[6]` wavefunction of gluon with color index, a
`cplx gb[6]` wavefunction of gluon with color index, b
`cplx gc[6]` wavefunction of gluon with color index, c (33)
`cplx gd[6]` wavefunction of gluon with color index, d
`float gg` coupling constant of VVV vertex

OUTPUTS:

`cplx vertex` amplitude of the VVVV vertex

The coupling constant `gg` for the $gggg$ vertex is

$$gg = g_s^2. \quad (34)$$

In order to obtain the complete amplitude, the function must be called three times (once for each color structure) with the following permutations:

$$\text{ggggxx}(\mathbf{ga}, \mathbf{gb}, \mathbf{gc}, \mathbf{gd}, \mathbf{gg}, \mathbf{v1}) \quad (35a)$$

$$\text{ggggxx}(\mathbf{ga}, \mathbf{gc}, \mathbf{gd}, \mathbf{gb}, \mathbf{gg}, \mathbf{v2}) \quad (35b)$$

$$\text{ggggxx}(\mathbf{ga}, \mathbf{gd}, \mathbf{gb}, \mathbf{gc}, \mathbf{gg}, \mathbf{v3}) \quad (35c)$$

The color amplitudes are then expressed as

$$f^{abe} f^{cde}(\mathbf{v1}) + f^{ace} f^{dbe}(\mathbf{v2}) + f^{ade} f^{bce}(\mathbf{v3}). \quad (36)$$

4.2.2 jgggx0

The HEGET function `jgggx0` (List 4 in Appendix) computes an off-shell gluon current from the four-point gluon coupling, including the gluon propagator in the Feynman gauge. It has the arguments:

$$\text{jgggx0}(\text{cplx* ga}, \text{cplx* gb}, \text{cplx* gc}, \text{float gg}, \text{cplx* jggg}) \quad (37)$$

where the inputs and the outputs are:

INPUTS:

`cmplx ga[6]` wavefunction of gluon with color index, a
`cmplx gb[6]` wavefunction of gluon with color index, b
`cmplx gc[6]` wavefunction of gluon with color index, c
`float gg` coupling constants of the VVVV vertex

OUTPUTS:

`cmplx jggg[6]` vector current $j^\mu(\mathbf{gd}; \mathbf{ga}, \mathbf{gb}, \mathbf{gc})$ which has a color index, d

(38)

The function (37) computes off-shell gluon wave function with three specific color index d which comes along with a specific color factor. As in eq. (35) it should be called three times

$$\text{jgggx0}(\mathbf{ga}, \mathbf{gb}, \mathbf{gc}, \mathbf{gg}, \mathbf{j1}) \quad (39a)$$

$$\text{jgggx0}(\mathbf{gc}, \mathbf{ga}, \mathbf{gb}, \mathbf{gg}, \mathbf{j2}) \quad (39b)$$

$$\text{jgggx0}(\mathbf{gb}, \mathbf{gc}, \mathbf{ga}, \mathbf{gg}, \mathbf{j3}) \quad (39c)$$

to give the off-shell gluon with the color factor

$$f^{abe} f^{cde}(\mathbf{j1}) + f^{ace} f^{dbe}(\mathbf{j2}) + f^{ade} f^{bce}(\mathbf{j3}). \quad (40)$$

5 Results

5.1 Comparison of total cross sections

In order to validate the new HEGET functions which are introduced in this report, we compare the total cross sections of n -jet production processes computed on the GPU with those calculated by other programs which are based on the FORTRAN version of the HELAS library. We use MadGraph/MadEvent [4] and another independent FORTRAN program which uses the Monte Carlo integration program, BASES [12], as references. Due to the limited support for the double precision computation capabilities on the GPU, the whole computations with HEGET on a GTX280 are done with single precision, while the other programs with HELAS in FORTRAN compute cross sections with double precision.

For the calculation of the n -jet production cross sections we use the same physics parameters as the MadGraph/MadEvent for all programs, and the same final state cuts of eq. (14) for all processes and all programs. The parton distribution functions of CTEQ6L1 [7] and the same factorization and renormalization scales, $Q = p_T^{\text{cut}} = 20\text{GeV}$, are also used.

Results for the computation of the total cross sections are summarized in Tables 6, 7 and 8 for $gg \rightarrow$ gluons, $u\bar{u} \rightarrow$ gluons and $uu \rightarrow uu +$ gluons, respectively. We find the results obtained by the HEGET functions agree with those from the other programs within the statistics of generated number of events.

We note that multi-jet events that satisfy the final state cuts of eq. (14), where all jets are in the central region in $|\eta| < 2.5$ (14a) and their transverse momentum about the beam direction (14b) and among each other (14c) greater than 20 GeV, are dominated by pure gluonic processes in Table 6. The cross sections for $u\bar{u} \rightarrow ng$ process in Table 7 are small because of $u\bar{u}$ annihilation. We note that the crossing-related non-annihilation processes, $ug \rightarrow u + (n-1)g$, have exactly the same number of diagrams and color bases, hence can be evaluated with essentially the same amount of computation time.

5.2 Comparison of the processing time

As already described in our previous report [1], we prepare two versions of the programs in the same structure for the computation of the total cross sections. One is written in CUDA, a C-based language, and can be executed on the GPU. The other is written in C and can be executed on the CPU. Using a standard C library function we measure the time between the start of the transfer of random numbers to the GPU and the end of the transfer of computed results back to the CPU.

In Fig. 1, the measured process time in μsec for one event of n -jet production processes is shown for the GPU (GTX280) and the CPU (Linux PC with Fedora 8). They are plotted against the number of jets in the final state. Because the process time per event on the GPU depends [1] strongly on the number of allocated registers at the compilation by the CUDA and the size of thread blocks at the execution time, we scan combination of these parameters for the fastest event process time on the GPU.

The upper three lines in Fig. 1 show the event process times on the CPU. They correspond to $gg \rightarrow n$ -jets denoted as \mathbf{gg} , $u\bar{u} \rightarrow n$ -jets as $\mathbf{u\bar{u}}$ and $uu \rightarrow uu + n$ -jets as \mathbf{uu} , respectively. For processes with small numbers of jets, e.g. $n_{\text{jet}} = 2$, the event process times for different processes are all around 4.5 μsec . This is probably because they are dominated by computation steps other than the amplitude calculations, such as computations of the PDF factors and the data transfer between GPU and CPU, which are common to all physics processes. When the number of jets becomes larger, the event process time for the same number jets in the final states is roughly proportional to the number of diagrams of each process listed in Table 1.

The lower three lines in Fig. 1 show the event process times on a GTX280. They also correspond to $gg \rightarrow n$ -jets denoted as \mathbf{gg} , $u\bar{u} \rightarrow n$ -jets as $\mathbf{u\bar{u}}$ and $uu \rightarrow uu + n$ -jets as \mathbf{uu} , respectively. As the number of jets becomes larger, the process time on the GPU grows more rapidly than that on the CPU. For the $n_{\text{jet}} = 4$ case, the event process time of $gg \rightarrow 4$ gluons is larger than the expected time from the proportionality to the number of diagrams of the other processes, $u\bar{u} \rightarrow 4$ gluons and $uu \rightarrow uu + 2$ gluons. In other words, the event process time on GPU grows faster than what we expect from the growth of the number of Feynman diagrams.

For instance, the event process times ratio for $gg \rightarrow 4g$ and $gg \rightarrow 3g$ on the CPU are roughly 120 $\mu\text{sec}/14 \mu\text{sec}$

Table 6. Total cross sections for $gg \rightarrow$ gluons [fb].

No. of jets	HEGET	Bases	MadGraph/MadEvent	
2	3.1929 ± 0.0010	3.1928 ± 0.0010	3.1902 ± 0.0076	$\times 10^{11}$
3	2.6201 ± 0.0023	2.6136 ± 0.0036	2.6221 ± 0.0061	$\times 10^{10}$
4	5.813 ± 0.020	5.8140 ± 0.0095	5.776 ± 0.034	$\times 10^9$

Table 7. Total cross sections for $u\bar{u} \rightarrow$ gluons [fb].

No. of jets	HEGET	Bases	MadGraph/MadEvent	
2	2.8981 ± 0.0007	2.8969 ± 0.0006	2.8991 ± 0.0073	$\times 10^7$
3	1.8420 ± 0.0012	1.8388 ± 0.0018	1.8421 ± 0.0077	$\times 10^6$
4	4.465 ± 0.022	4.496 ± 0.017	4.399 ± 0.038	$\times 10^5$
5	1.566 ± 0.057	1.589 ± 0.018	1.542 ± 0.039	$\times 10^5$

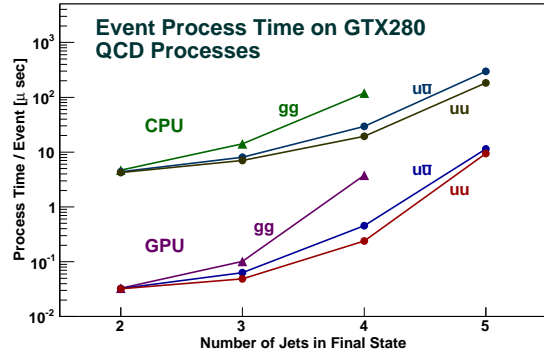
Table 8. Total cross sections for $uu \rightarrow uu +$ gluons [fb].

No. of jets	HEGET	Bases	MadGraph/MadEvent	
2	2.6715 ± 0.0014	2.6743 ± 0.0011	2.6689 ± 0.0047	$\times 10^8$
3	5.897 ± 0.004	5.889 ± 0.010	5.871 ± 0.015	$\times 10^7$
4	2.7754 ± 0.0130	2.7500 ± 0.0083	2.748 ± 0.042	$\times 10^7$
5	1.513 ± 0.024	1.560 ± 0.013	1.513 ± 0.024	$\times 10^6$

~ 8.6 , which roughly agrees with the ratio of the numbers of Feynman diagrams (Table 1), $510/45 \sim 11$. The corresponding ratio on GPU is $3.8 \mu\text{sec}/0.1 \mu\text{sec} \sim 38$, which is significantly larger.

For the same number of jets, we also observe that the event process times on the CPU are roughly proportional to the number of diagrams. For $n_{\text{jet}} = 4$, the ratio of the process times for $gg \rightarrow 4g$ to $u\bar{u} \rightarrow 4g$ are about $120 \mu\text{sec}/29 \mu\text{sec} \sim 4.1$ on CPU, as compared to the ratio of the number of Feynman diagrams in Table 1, $510/159 \sim 3.2$. The same applies to $n_{\text{jet}} = 5$ between $u\bar{u} \rightarrow 5g$ and $uu \rightarrow uuggg$, where Feynman diagrams have the ratio $1890/786 \sim 2.4$ from Table 1, and the event process time on the CPU gives $300 \mu\text{sec}/180 \mu\text{sec} \sim 1.7$, also in rough agreement.

On the other hand, the event process times on the GPU for $gg \rightarrow 4g$ and $u\bar{u} \rightarrow 4g$ have a ratio $3.8 \mu\text{sec}/0.45 \mu\text{sec} \sim 8.4$ which is much larger than the ratio of the diagram numbers; while that for $u\bar{u} \rightarrow 5g$ and $uu \rightarrow uuggg$ has the ratio of $11 \mu\text{sec}/9.5 \mu\text{sec} \sim 1.15$. Although we do not fully understand the above behavior of the event process time on the GPU, we find that they tend to scale as the product of the number of Feynman diagrams and the number of color bases, while the event process times on the CPU are not sensitive to the latter. This is probably because as the number of color bases grows, more amplitudes, $(J_{\lambda_i})_{\alpha}$ in eq. (8), should be stored and then called to compute the color sum, eq. (10). These observations tell us that the relative weight of the color matrix computation in the GPU computing is very significant even after identifying the independent elements of the color matrix $\mathcal{N}_{\alpha\beta}$ in eq. (9) as listed in Table 4.

**Fig. 1.** Processing time for GPU and CPU.

5.3 Comparison of performance of GPU and CPU

The ratios of event process times between CPU and GPU are shown in Fig. 2. Three lines correspond to $gg \rightarrow n$ -jets denoted as **gg**, $u\bar{u} \rightarrow n$ -jets as **uū** and $uu \rightarrow uu + (n-2)$ -jets as **uu**, respectively. The performance ratios exceed 100 for the processes with small numbers of jets ($n_{\text{jet}} \leq 3$) in the final state. For $n_{\text{jet}} = 4$ and 5, the performance ratios gradually drop to less than 40. For processes with large numbers of color bases, the ratios are smaller. For $gg \rightarrow 4$ gluons, which has 120 color bases, the ratio is about 30, and for $uu \rightarrow uu + 3$ gluons, which has 240 color bases, the ratio becomes about 20.

5.4 Note on $gg \rightarrow 5g$ study

Among five-jet production processes we have not been able to run the program for $gg \rightarrow 5g$. This process has 7245 di-

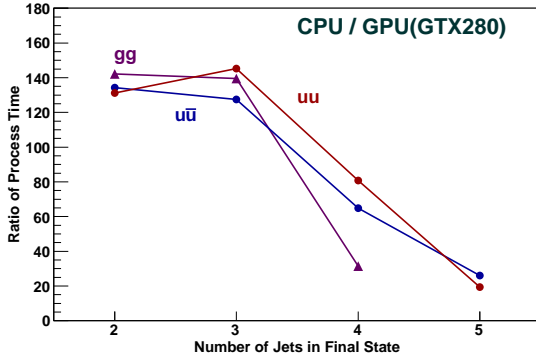


Fig. 2. Ratio of processing time. Time on CPU divided by time on GPU.

agrams and 720 color basis vectors. In order to compile the program for the computation of this process, we use the technique developed in the previous study [1]. By dividing the program into about 140 pieces we were able to compile the $gg \rightarrow 5g$ program. Compilation takes about 90 min. on a Linux PC. The total size of the compiled program exceeds 200 MB, and we were not able to execute this compiled program on a GTX280.

6 Summary

We have shown the results of our attempt to evaluate QCD multi-jet production processes at hadron colliders on a GPU [11], Graphic Processing Unit, following the encouraging results obtained for QED multi-photon production processes in ref. [1].

Our achievements and findings may be summarized as follows.

- A new set of HEGET functions written in CUDA [2], a C-language platform developed by NVIDIA for general purpose GPU computing, are introduced to compute triple and quartic gluon vertices. The HEGET routines for massless quarks were introduced in ref. [1], and the routine for photons [1] can be used for gluons. In addition, the HEGET functions for the qqg vertex are the same as those for the $qq\gamma$ vertex introduced in ref. [1].
- The HELAS amplitude code generated by MadGraph [4] is converted to a CUDA program which calls HEGET functions for the following three type of subprocesses: $gg \rightarrow ng$ ($n \leq 5$), $u\bar{u} \rightarrow ng$ ($n \leq 5$), and $uu \rightarrow uu + ng$ ($n \leq 3$).
- Summation over color degrees of freedom was performed on a GPU by identifying the same valued elements of the color matrix of eq. (9), in order to reduce the memory size.
- All the HEGET programs for up to 5 jets passed the CUDA compiler after division into small pieces. However, we could not execute the program for the process $gg \rightarrow 5g$. Accordingly, comparisons of performance be-

tween GPU and CPU are done for the multi-jet production processes up to 5 jets, excluding the purely gluonic subprocess.

- Event process times of the GPU program on GTX280 are more than 100 times faster than the CPU program for all the processes up to 3-jets, while the gain is reduced to 60 for 4-jets with one or two quark lines, and to 30 for the purely gluonic process. It further goes down to 30 and 20 for 5-jet production processes with one and two quark lines, respectively.
- We find that one cause of the rapid loss of GPU gain over CPU as the number of jets increases is the growth in the number of color bases. GPU programs slow down for processes with larger numbers of color basis vectors, while the performance of the CPU programs is not affected much.
- All computations on the GPU were performed with single precision accuracy. A factor of 2.5 to 4 slower performance is found for double precision computation on the GPU.

Acknowledgement. We thank Johan Alwall, Qiang Li and Fabio Maltoni for stimulating discussions. This work is supported by the Grant-in-Aid for Scientific Research from the Japan Society for the Promotion of Science (No. 20340064) and the National Science Foundation (No. 0757889).

Appendix A Additional HEGET functions

In the appendix, we list the HEGET functions introduced in this report. They are for the ggg and $gggg$ vertices which do not have counterparts in QED. Together with the HEGET functions listed in ref. [1], the quark and gluon (photon) wave functions and the $qqg(qq\gamma)$ vertices, all the QCD amplitudes can be computed on GPU.

Appendix A.1 Functions for the VVV vertex

List 1. vvvxxx.cu

```
#include "cmplx.h"
__device__
void vvvxxx(cmplx* ga, cmplx* gb, cmplx* gc,
            float g, cmplx* vertex)
{
    cmplx v12 = ga[0]*gb[0]
              - ga[1]*gb[1] - ga[2]*gb[2] - ga[3]*gb[3];
    cmplx v23 = gb[0]*gc[0]
              - gb[1]*gc[1] - gb[2]*gc[2] - gb[3]*gc[3];
    cmplx v31 = gc[0]*ga[0]
              - gc[1]*ga[1] - gc[2]*ga[2] - gc[3]*ga[3];

    float pga[4];
    float pgb[4];
    float pgc[4];

    pga[0] = ga[4].re;
    pga[1] = ga[5].re;
    pga[2] = ga[5].im;
    pga[3] = ga[4].im;

    pgb[0] = gb[4].re;
    pgb[1] = gb[5].re;
    pgb[2] = gb[5].im;
    pgb[3] = gb[4].im;
```



```

pgc[0] = gc[4].re;
pgc[1] = gc[5].re;
pgc[2] = gc[5].im;
pgc[3] = gc[4].im;

cplx p12 = pga[0]*gb[0]
- pga[1]*gb[1] - pga[2]*gb[2] - pga[3]*gb
  [3];
cplx p13 = pga[0]*gc[0]
- pga[1]*gc[1] - pga[2]*gc[2] - pga[3]*gc
  [3];
cplx p21 = pgb[0]*ga[0]
- pgb[1]*ga[1] - pgb[2]*ga[2] - pgb[3]*ga
  [3];
cplx p23 = pgb[0]*gc[0]
- pgb[1]*gc[1] - pgb[2]*gc[2] - pgb[3]*gc
  [3];
cplx p31 = pgc[0]*ga[0]
- pgc[1]*ga[1] - pgc[2]*ga[2] - pgc[3]*ga
  [3];
cplx p32 = pgc[0]*gb[0]
- pgc[1]*gb[1] - pgc[2]*gb[2] - pgc[3]*gb
  [3];

vertex = -(v12*(p13-p23)
+ v23*(p21-p31)
+ v31*(p32-p12))*g;

return;
}

```

List 2. jvxxx0.cu

```

#include "cplx.h"
__device__
void jggxxx(cmplx* ga, cmplx* gb, float g,
  cmplx* jvv)
{
  jvv[4] = ga[4] + gb[4];
  jvv[5] = ga[5] + gb[5];

  float p1[4];
  float p2[4];
  float q[4];

  p1[0] = (ga[4].re);
  p1[1] = (ga[5].re);
  p1[2] = (ga[5].im);
  p1[3] = (ga[4].im);

  p2[0] = (gb[4].re);
  p2[1] = (gb[5].re);
  p2[2] = (gb[5].im);
  p2[3] = (gb[4].im);

  q[0] = -(jvv[4].re);
  q[1] = -(jvv[5].re);
  q[2] = -(jvv[5].im);
  q[3] = -(jvv[4].im);

  float s = q[0]*q[0]-q[1]*q[1]-q[2]*q[2]-q[3]*q
    [3];

  cplx gab = ga[0]*gb[0]
- ga[1]*gb[1] - ga[2]*gb[2] - ga[3]*gb[3];

  cplx sga = (p2[0]-q[0])*ga[0] - (p2[1]-q[1])*
    ga[1]
- (p2[2]-q[2])*ga[2] - (p2[3]-q[3])*ga[3];

  cplx sgb = -(p1[0]-q[0])*gb[0] + (p1[1]-q[1])*
    gb[1]
+ (p1[2]-q[2])*gb[2] + (p1[3]-q[3])*gb[3];

  float gs = -g*(1.0f/s);

  jvv[0] = gs*((p1[0]-p2[0])*gab
+ sga*gb[0] + sgb*ga[0]);
  jvv[1] = gs*((p1[1]-p2[1])*gab
+ sga*gb[1] + sgb*ga[1]);
  jvv[2] = gs*((p1[2]-p2[2])*gab
+ sga*gb[2] + sgb*ga[2]);
  jvv[3] = gs*((p1[3]-p2[3])*gab
+ sga*gb[3] + sgb*ga[3]);

  return;
}

```

Appendix A.2 Functions for the VVVV vertex

List 3. ggggxx.cu

```

#include "cplx.h"
__device__
void ggggxx(cmplx* ga, cmplx* gb, cmplx* gc,
  cmplx* gd, float gg, cmplx* vertex)
{
  cplx gad = ga[0]*gd[0]
- ga[1]*gd[1]-ga[2]*gd[2]-ga[3]*gd[3];

  cplx gbc = gb[0]*gc[0]
- gb[1]*gc[1]-gb[2]*gc[2]-gb[3]*gc[3];

  cplx gac = ga[0]*gc[0]
- ga[1]*gc[1]-ga[2]*gc[2]-ga[3]*gc[3];

  cplx gbd = gb[0]*gd[0]
- gb[1]*gd[1]-gb[2]*gd[2]-gb[3]*gd[3];

  vertex = gg*(gad*gbg-gac*gbd);

  return;
}

```

List 4. jgggx0.cu

```

#include "cplx.h"
__device__
void jgggx0(cmplx* ga, cmplx* gb, cmplx* gc,
  float gg, cmplx* jggg)
{
  jggg[4] = ga[4]+gb[4]+gc[4];
  jggg[5] = ga[5]+gb[5]+gc[5];

  float q[4];
  q[0] = -jggg[4].re;
  q[1] = -jggg[5].re;
  q[2] = -jggg[5].im;
  q[3] = -jggg[4].im;

  float fact = gg*(1.0f/(q[0]*q[0]
- q[1]*q[1]-q[2]*q[2]-q[3]*q
  [3]));

  cplx gcb = gc[0]*gb[0]
- gc[1]*gb[1]-gc[2]*gb[2]-gc[3]*gb[3];
  cplx gac = ga[0]*gc[0]
- ga[1]*gc[1]-ga[2]*gc[2]-ga[3]*gc[3];

  jggg[0] = fact*( ga[0]*gcb - gb[0]*gac );
  jggg[1] = fact*( ga[1]*gcb - gb[1]*gac );
  jggg[2] = fact*( ga[2]*gcb - gb[2]*gac );
  jggg[3] = fact*( ga[3]*gcb - gb[3]*gac );

  return;
}

```

References

1. K. Hagiwara, J. Kanzaki, N. Okamura, D. Rainwater and T. Stelzer, arXiv:0908.4403.
2. http://www.nvidia.com/object/cuda_home.html
3. K. Hagiwara, H. Murayama and I. Watanabe, Nucl. Phys. **B367** (1991) 257; H. Murayama, I. Watanabe and K. Hagiwara, KEK-Report 91-11, 1992.
4. T. Stelzer and W. F. Long, Comput. Phys. Commun. **81** (1994) 357.
5. See e.g. M.L. Mangano and S.J. Parke, Phys. Rept. **200**, 301 (1991).
6. S. Catani, Y.L. Dokshitzer, M.H. Seymour, B.R. Webber, Nucl. Phys. **B406**, 187 (1993)

7. CTEQ Collaboration, H.L. Lai et al., Eur. Phys. J. **C12** (2000) 375.
8. C. Amsler et al. (Particle Data Group), Phys. Lett. **B667**, 1 (2008) and 2009 partial update for the 2010 edition.
9. F. Maltoni and T. Stelzer, JHEP **0302** (2003) 027.
10. J. Alwall, P. Demin, S. de Vissher, R. Frederix, M. Herquet, F. Maltoni, T. Plehn, D. Rainwater, T. Stelzer, JHEP **0709** (2007) 028.
11. <http://www.nvidia.com/page/home.html>
12. S. Kawabata, Comput. Phys. Commun. **41**(1986) 127.
13. H. Plochow-Besch, Comput. Phys. Commun. **75** (1993) 396, Int. J. Mod. Phys. **A10** (1995) 2901.